(Received 24 May 2025, Accepted 1 July 2025, Scheduled 16 July 2025)

Miniaturized Broadband Dielectric Waveguide Resonator Bandpass Filter with Wide Stopband Using CPW Resonator

Chuanyun Wang[1,2], Hao Huang[1,2], and Pin Wen[1,2,*]

[1]School of Information and Software Engineering, East China Jiaotong University, Nanchang 330013, China
[2]School of Information Engineering, Nanchang University, Nanchang 330031, China

ABSTRACT: In this paper, a novel miniaturized broadband dielectric waveguide (DW) bandpass filter (BPF) with wide stopband response is proposed. The proposed BPF is composed of two square DW resonators operating in TM_{101} mode. By etching a coplanar waveguide (CPW) resonator on a silver-plated metal surface in the middle of the two DW resonators, an additional resonant mode is introduced, thereby broadening the bandwidth of the filter while retaining the inherent advantages of the DW structure. Simultaneously, the CPW resonator creates a new coupling path that enables cross-coupling and introduces a controlled transmission zero (TZ). The position of the TZ can be adjusted to suppress the second harmonic of the filter, ensuring effective stopband performance. For verification, a DW BPF with center frequency of 5 GHz and a fractional bandwidth of 11.4% was designed, fabricated, and measured. The measured results are in excellent agreement with the simulated ones. Specifically, the upper stopband of the filter extends to twice of the center frequency (10 GHz), demonstrating the wide stopband characteristics of the filter.

1. INTRODUCTION

Filtering circuits play an important role in the radio frequency front ends of the wireless communication systems. Printed circuit board (PCB) microstrip resonators have been popular in filter circuit designs for decades due to their advantages of compact size and light weight [1–4]. However, microstrip filters show the disadvantage of relatively high insertion loss (IL) because of the low external quality factor of the microstrip resonator. Furthermore, both metal coaxial resonators and dielectric resonators have garnered significant attention from researchers, primarily attributable to their high unloaded quality factors. Metal coaxial resonators have been widely applied in bandpass filters (BPFs) designs for base stations [5–7], while dielectric resonator filters have been employed in satellite and base station applications [8, 9]. However, the size of the circuits of the metal coaxial cavity occupies tremendous volume, and the size of the DR-loaded metal cavity filter is generally large due to the metal shielding box. This results in poor space efficiency. For applications in 5G communication systems, BPFs are required to have low IL, light weight, and small size [10]. Additionally, broadband response and wide stopband characteristics are key development directions for 5G base station filters. Accordingly, dielectric waveguide resonators (DWRs) have received increasing attention due to their high Q-factor, high relative permittivity, low IL, good temperature stability, and compact size [11, 12, 14–18, 21, 22].

In [11] and [12], electrical coupling is introduced by integrating a PCB with a DWR, and electromagnetic hybrid coupling is used to generate transmission zeros (TZs). However, the introduction of an additional PCB structure leads to significant degradation of IL and dimensional performance. In [14] and [16], traditional magnetic coupling is used between DWRs, and cross-coupling is introduced to generate TZs. However, these approaches generally result in narrow bandwidths and relatively poor bandstop performance. Therefore, it is necessary to study DWR filters that meet the requirements of broadband operation, wide stopband, and miniaturization simultaneously.

This work proposes a novel DWR filter using coplanar waveguide (CPW) technology. A CPW resonator is formed by etching slotlines on a silver-plated layer positioned in the middle of the two DWRs, creating an additional resonance and introducing cross-coupling. This design broadens the bandwidth of the filter without increasing its size. Moreover, the cross-coupling creates a controllable TZ in the upper band, and a wide stopband effect is achieved by adjusting TZ position to suppress the second harmonic. To validate the design, a miniaturized broadband DWR filter with a wide stopband response was fabricated and measured. The results demonstrate excellent performance and meet the requirements of applications such as 5G and satellite communication.

2. RESONATOR AND MODE ANALYSIS

Figure 1(a) shows the structure of a silver-plated square DWR with dimensions of $a \times a \times h$, using a dielectric with a relative permittivity of 20.3 and a loss tangent of 1.5×10^{-4}.

The electric filed (E-field) distribution of the TM_{101} mode in the DWR is shown in Fig. 1(b). The frequency of modes can be calculated by [13]

$$f_{\mathrm{TM}_{m0n}} = \frac{c}{2\pi\sqrt{\varepsilon_r}}\sqrt{\left(\frac{m\pi}{a}\right)^2 + \left(\frac{n\pi}{b}\right)^2} \tag{1}$$

* Corresponding author: Pin Wen (wenpin925@hotmail.com).

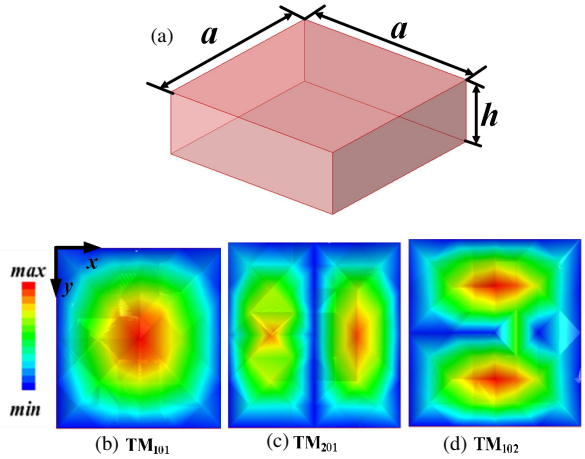

FIGURE 1. (a) 3D view of the square DWR. (b), (c) and (d) are E-field distributions of TM_{101}, TM_{201} and TM_{102} mode, respectively.

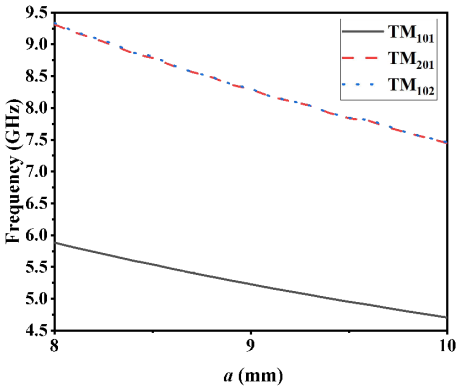

FIGURE 2. Resonant frequency versus length of the DWR.

where c is the speed of light; ε_r is the relative permittivity; a and b are the length and width of DWR, respectively. TM_{201} and TM_{102} modes are the higher-order modes of DWR, with their E-field distributions shown in Figs. 1(c) and (d). The frequency of the modes can be calculated by formula (1). These two modes are a pair of degenerate modes which together form a second harmonic. Fig. 2 illustrates the relationship between the length of DWR and the resonant frequency variation for each mode. The center frequency of the proposed filter can be adjusted by changing a. Additionally, the frequency of the second harmonic is determined to serve as a reference for subsequent wide stopband design.

3. ANALYSIS AND DESIGN OF THE PROPOSED FILTER

The magnetic field (M-field) distribution of the square DWR operating in TM_{101} mode is depicted in Fig. 3(a). Magnetic coupling is effectively introduced by connecting the two TM_{101} resonant cavities through the coupling window, where the M-field is the strongest.

As depicted in Fig. 3(b), a novel cross-coupling structure is proposed by etching two slotlines on the silver-plated layer to form a CPW resonator. This CPW resonator connects the central regions of the two DWRs, where the E-field is maximized. The CPW resonator functions as an additional resonator to form a third-order filter with two DWRs, thereby expanding the operating bandwidth of the filter without increasing its size. This design results in a more compact filter structure. Fig. 3(c) illustrates the EM-field distribution of the entire filter operating in TM_{101} mode after connecting two square DWRs through the coupling window and further loading the CPW resonator. Magnetic coupling is successfully introduced by connecting the two square DWRs through the coupling window, where the M-field is the strongest in the TM_{101} mode. Meanwhile, electric coupling is introduced between the two resonant cavities via the loaded CPW structure, achieving mixed EM coupling.

Figure 4 illustrates the topology of the proposed DWR filter. The CPW is connected to the maximum E-field in the two DWRs, thereby establishing electric coupling between the DWR and CPW resonator. Additionally, magnetic coupling between the two DWRs is achieved through the coupling window, which facilitates cross-coupling. This cross-coupling introduces a TZ into the response of the filter.

The use of the CPW structure does not degrade the inherent advantages of DWR. As shown in Fig. 5, when the DWR filter operates in the fundamental TM_{101} mode, the current direction around the CPW is essentially parallel to the slotlines, resulting in minimal current interruption. Consequently, there is negligible radiation loss and no degradation of the structural shielding or quality factor.

As a design procedure, a third-order BPF at the center frequency of 5 GHz was synthesized. It exhibits a return loss (RL) of 20 dB, a TZ at 8 GHz, and a fractional bandwidth (FBW) of 11.4%. The coupling matrix M of the proposed filter can be synthesized as

$$[M]=\begin{bmatrix} & S & 1 & 2 & 3 & L \\ S & 0 & 0.558 & 0 & 0 & 0 \\ 1 & 0.558 & 0 & 0.482 & -0.658 & 0 \\ 2 & 0 & 0.482 & 0 & 0.482 & 0 \\ 3 & 0 & -0.658 & 0.482 & 0 & 0.558 \\ L & 0 & 0 & 0 & 0.558 & 0 \end{bmatrix} \quad (2)$$

where the negative values represent the inductive couplings, and the positive values are the capacitive couplings.

The external quality factor Q_e of the DWR TM_{101} mode can be determined based on the desired FBW using formula (3) [19].

$$Q_e = \frac{1}{\text{FBW} \cdot M_{S1}^2} \quad (3)$$

Figure 6(a) illustrates the trend of the external quality factor Q_e of the resonant mode in relation to the length h_1 of the feeding probe. As the length h_1 increases, Q_e gradually increases. Therefore, the Q_e of the TM_{101} mode can be easily controlled to obtain the desired value.

In order to achieve the regulation of the TZ position, the parameters related to the cross-coupling are analysed next. The effect of the coupling window size on the coupling coefficients k for primary and cross coupling is shown in Figs. 6(b) and (c). In the coupled structure, the coupling window length d and width w have significant impacts on the coupling strength between the resonators. Specifically, as the coupling window

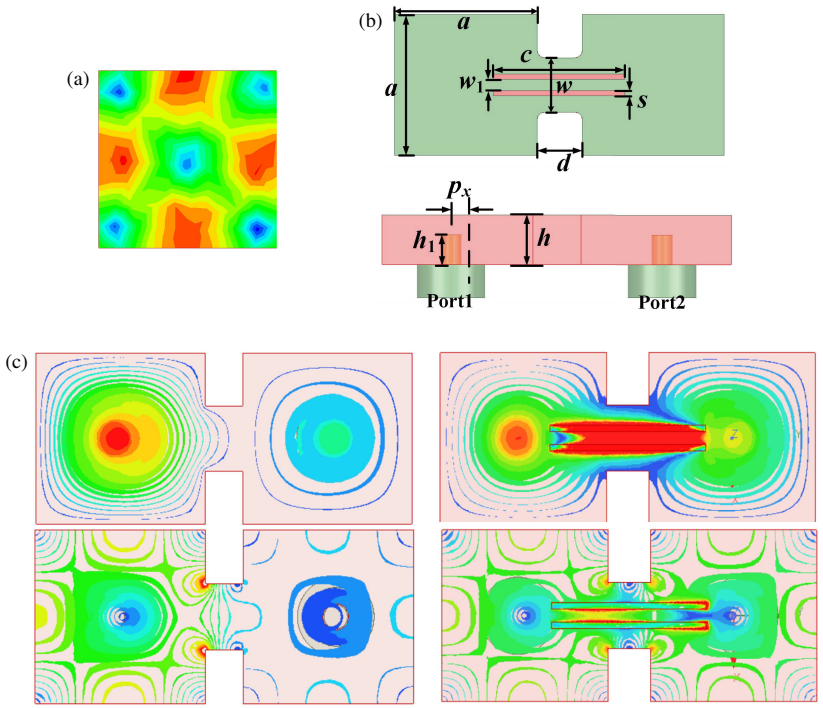

FIGURE 3. (a) M-field distribution of the TM_{101} mode of the square DWR. (b) Structure of the proposed third-order DWR filter. (c) EM-field distribution of the overall filter operating in TM_{101} mode after connecting two square DWR through the coupling window and further loading the CPW structure.

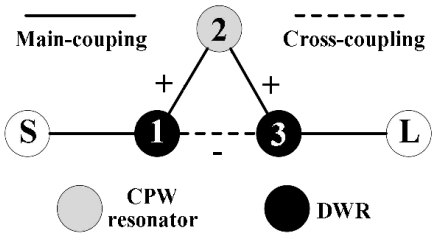

FIGURE 4. Coupling topology of the filter.

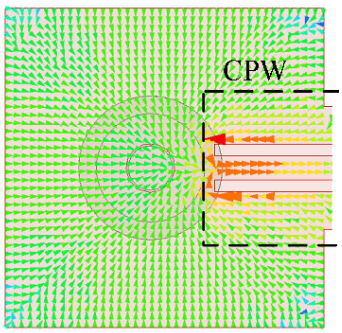

FIGURE 5. Surface current of a DWR working in TM_{101}.

length d increases, the coupling strength between the resonators weakens, which results in a monotonic decrease in the coupling coefficients. Conversely, when the width of the coupling window w increases, the energy coupling between the resonators is enhanced, thereby leading to an increase in the coupling coefficients. By controlling the size of the coupling window, the inter-cavity coupling coefficients can be easily adjusted.

The position of the TZs introduced by cross coupling can be controlled by the coupling strength between the resonators. The frequency of the TZ can be approximated by [20]

$$f_z = f_0 \sqrt{\frac{k_m}{|k_e|}} \tag{4}$$

where f_z is the frequency of the TZ; f_0 is the centre frequency of the filter; k_m and k_e are the magnetic and electric coupling coefficients of the filter, respectively. In Fig. 6, k_{12} and k_{23} denote the electric coupling between the CPW resonators and DWRs, and k_{13} denotes the magnetic coupling between the DWRs. From the figure, it can be seen that when the length of the coupling window d increases, the decrease of the electric coupling coefficient is much larger than the magnetic coupling coefficient, thus the f_z in formula (4) gradually increases, and the TZ moves to the high frequency; when the width of the coupling window w increases, the increase of the electric coupling coefficient is much larger than the magnetic coupling coefficient, thereby the f_z in formula (4) gradually decreases, and the TZ moves to the low frequency. Therefore, the coupling coefficients between the resonators, and consequently the position of the TZ, can be controlled by adjusting the size of the coupling window.

Figure 7 shows the simulated responses that vary with the length d and width w of the coupling window. In Fig. 7(a), as d increases, the TZ moves to a higher frequency. In Fig. 7(b), as w increases, the TZ moves to a lower frequency. This result

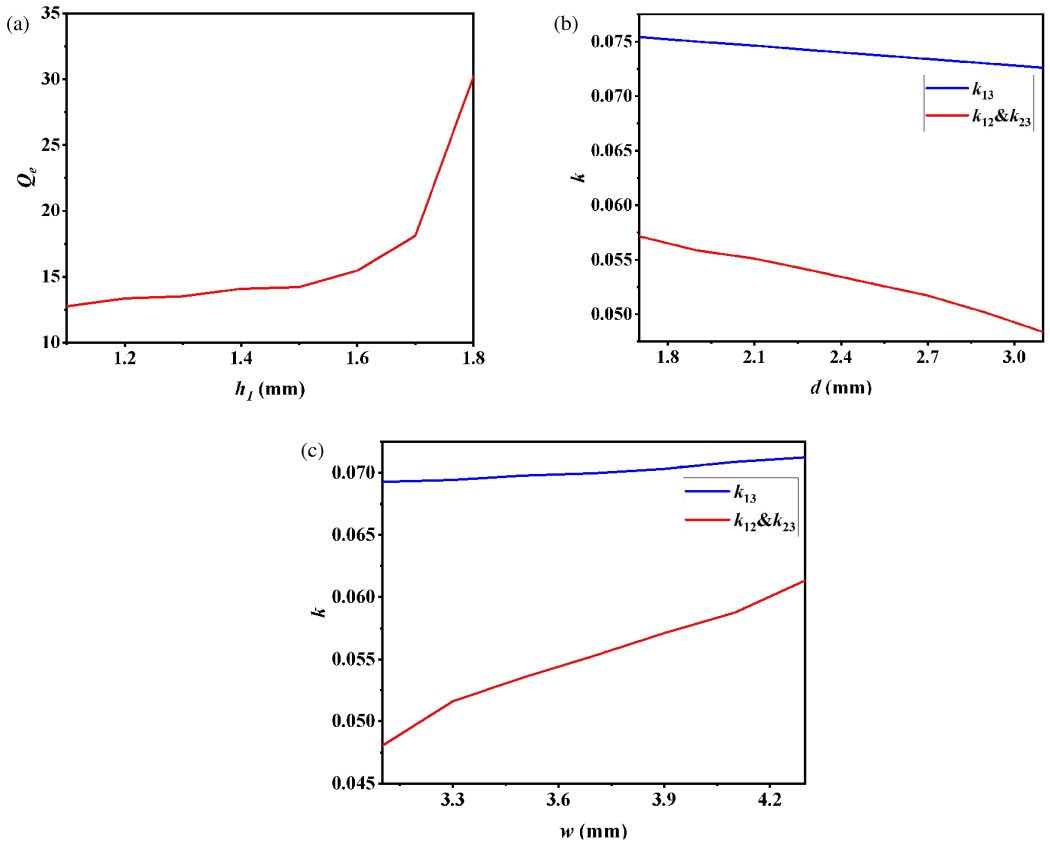

FIGURE 6. (a) Q_e versus the length h_1 of the feeding probe and coupling coefficients k versus (b) the length d of the coupling window and (c) the width w of the coupling window.

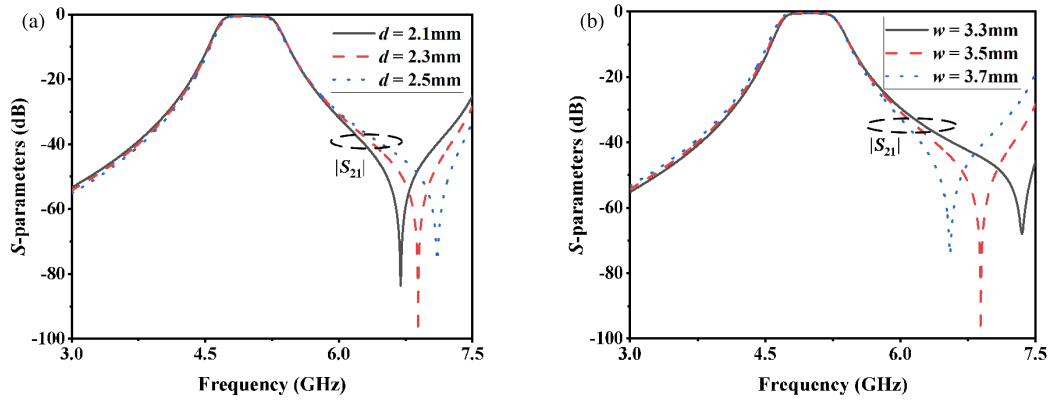

FIGURE 7. (a) Simulation S_{21} with different coupling window lengths d and (b) widths w of the coupling window.

proves the correctness of the cross-coupled TZ control method. By appropriately adjusting the position of the TZ, the second harmonic of the filter can be effectively suppressed, thereby achieving wide stopband performance.

4. FILTER IMPLEMENTATION AND RESULTS

To verify the proposed theory, a miniaturized broadband wide stopband BPF with a center frequency of 5 GHz is simulated, processed, and measured. The filter was designed by etching a CPW resonator on a silver-plated surface positioned between two square DWR resonators.

Figure 8 illustrates the configuration and physical prototype of the designed BPF. The DWR uses a silver-plated ceramic with a permittivity $\varepsilon_r = 20.3$. Insert the 50 Ω SMA feed probe into the two feed blind holes at the bottom of the DWR to perform external coupling feeding of the filter. The parameters of the filter were optimised to achieve the stated objectives, and the final geometry obtained was: $a = 9.1$, $h = 3$, $d = 2.9$, $w = 3.5$, $p_x = 0.5$, $h_1 = 1.8$, $c = 8.5$, $w_1 = 0.73$ and $s = 0.34$ (unit: mm), where p_x is the offset of the feed port from the center of the square DWR. The simulated and measured results of the proposed miniaturized wide stopband DWR filter are ob-

TABLE 1. Measured results in comparison with previously BPFs.

Ref.	f_0 (GHz)	Filter Order	IL (dB)	RL (dB)	FBW (%)	Circuit Size (λ_g^3)	Rejection Level	Type
[10]	2.7	4	0.26	20	1.2	$0.315 \times 0.315 \times 0.405$ $(0.04\lambda_g^3)$	$20/1.2f_0$	DR
[11]	2.6	4	0.6	20	6	$0.47 \times 0.23 \times 0.07$ $(0.0076\lambda_g^3)$	$30/1.23f_0$	DWR+PCB
[12]	3.45	4	0.8	19	2.9	$0.41 \times 0.32 \times 0.07$ $(0.0092\lambda_g^3)$	$20/1.1f_0$	DWR+PCB
[14]	3.5	4	< 1	> 18	5.7	$0.42 \times 0.21 \times 0.05$ $(0.0044\lambda_g^3)$	$20/ < 1.26f_0$	DWR
[17]	3.99/4.33	2	0.56/0.24	> 14	2/2.54	$0.29 \times 0.13 \times 0.13$ $(0.0049\lambda_g^3)$	$20/1.23f_2$	DWR
This work	4.98	3	0.63	20	13	$0.36 \times 0.15 \times 0.05$ $(0.0027\lambda_g^3)$	$20/2f_0$	DWR

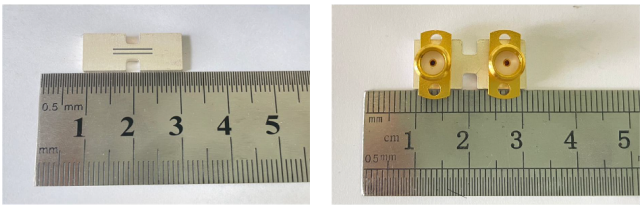

FIGURE 8. Photograph of the manufactured DWR BPF with wide stopband using CPW resonator.

tained by using Ansoft HFSS and a vector network analyzer (VNA).

After fine-tuning the parameters, the final simulated and measured results are shown in Fig. 9. The measured result accords well with the simulated result. The passband ranges from 4.65 GHz to 5.3 GHz, with center frequency at 4.98 GHz and FBW of 13%. The measured in-band RL is better than 20 dB, and the in-band IL is only 0.63 dB. The stopband rejection level of 20 dB up to $2f_0$ is achieved. Due to the inevitable dimensional deviation in processing and the sensitivity of the TZ to the filter dimensions, the position of the measured TZ deviates slightly from the simulation results, which reduces the stopband rejection effect of the filter. Table 1 displays the comparisons with other dielectric filters. The results show that the proposed DWR filter achieves a wider bandwidth and broader stopband performance with the smallest circuit size.

5. CONCLUSION

In this paper, a novel broadband miniaturized DWR BPF with a wide stopband response is proposed. By etching two slotlines on the silver-plated metal surface located between two square DWRs, a CPW resonator is formed. The CPW resonator introduces a new pole in the passband without increasing the size of the filter, thereby broadening the bandwidth while enabling the miniaturization of the filter. Additionally, the cross-coupling of the filter is realized through the introduction of the CPW

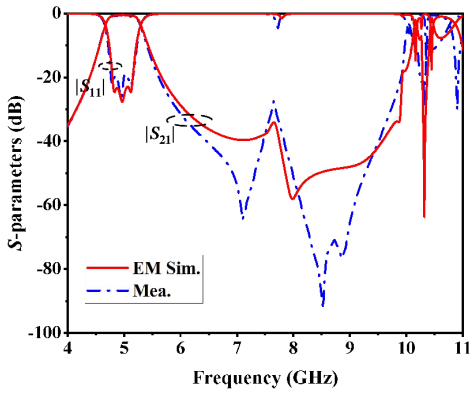

FIGURE 9. EM simulated and measured results of the proposed miniaturized wide stopband BPF.

resonator, which generates a controllable TZ in the upper frequency band. By adjusting the position of the TZ, the second harmonic is effectively suppressed, resulting in good stopband performance. Finally, a miniaturized broadband wide stopband DWR BPF with center frequencies of 5 GHz and FBW of 11.4% is designed and fabricated. The simulated and measured results of this filter are compared to verify our proposed structure. The filter has direct application potential in 5G infrastructure, satellite communications, and military applications.

ACKNOWLEDGEMENT

This work is funded by the National Natural Science Foundation of China (No. 61901170), the Department of Education Science and Technology Program of Jiangxi Province (Nos. GJJ2200609, GJJ2200622) and the Jiangxi Province Key Research and Development Plan (No. 20243BBG71030).

REFERENCES

[1] Hsu, H.-W., C.-H. Lai, and T.-G. Ma, "A miniaturized dual-mode ring bandpass filter," *IEEE Microwave and Wireless Components Letters*, Vol. 20, No. 10, 542–544, Oct. 2010.

[2] Tang, J., H. Liu, and Y. Yang, "Compact wide-stopband dual-band balanced filter using an electromagnetically coupled SIR pair with controllable transmission zeros and bandwidths," *IEEE Transactions on Circuits and Systems II: Express Briefs*, Vol. 67, No. 11, 2357–2361, Nov. 2020.

[3] Kim, C. H. and K. Chang, "Wide-stopband bandpass filters using asymmetric stepped-impedance resonators," *IEEE Microwave and Wireless Components Letters*, Vol. 23, No. 2, 69–71, Feb. 2013.

[4] Belyaev, B. A., A. M. Serzhantov, A. A. Leksikov, Y. F. Bal'va, and A. A. Leksikov, "Novel high-quality compact microstrip resonator and its application to bandpass filter," *IEEE Microwave and Wireless Components Letters*, Vol. 25, No. 9, 579–581, Sep. 2015.

[5] Wang, Y. and M. Yu, "True inline cross-coupled coaxial cavity filters," *IEEE Transactions on Microwave Theory and Techniques*, Vol. 57, No. 12, 2958–2965, Dec. 2009.

[6] Doumanis, E., "A technique to suppress harmonic outputs in coaxial cavity filters at the excitation port," *IEEE Microwave and Wireless Components Letters*, Vol. 26, No. 11, 876–878, Nov. 2016.

[7] Zhang, Z.-C., X.-Z. Yu, S.-W. Wong, B.-X. Zhao, J.-Y. Lin, X. Zhang, and K.-W. Tam, "Miniaturization of triple-mode wideband bandpass filters," *IEEE Transactions on Components, Packaging and Manufacturing Technology*, Vol. 12, No. 8, 1368–1374, Aug. 2022.

[8] Panariello, A., M. Yu, and C. Ernst, "Ku-band high power dielectric resonator filters," *IEEE Transactions on Microwave Theory and Techniques*, Vol. 61, No. 1, 382–392, Jan. 2013.

[9] Memarian, M. and R. R. Mansour, "Quad-mode and dual-mode dielectric resonator filters," *IEEE Transactions on Microwave Theory and Techniques*, Vol. 57, No. 12, 3418–3426, Dec. 2009.

[10] Pang, X., W. Hong, T. Yang, and L. Li, "Design and implementation of an active multibeam antenna system with 64 RF channels and 256 antenna elements for massive MIMO application in 5G wireless communications," *China Communications*, Vol. 11, No. 11, 16–23, Nov. 2014.

[11] Qin, W., J. Liu, H.-L. Zhang, W.-W. Yang, and J.-X. Chen, "Bandpass filter and diplexer based on dual-mode dielectric filled waveguide resonators," *IEEE Access*, Vol. 10, 29 333–29 340, 2022.

[12] Qin, W., J. Liu, W.-W. Yang, J.-X. Chen, Y. Li, and R.-L. Xu, "Integrated-designs of filtering circuits based on adjustable dielectric waveguide resonators," *IEEE Transactions on Circuits and Systems II: Express Briefs*, Vol. 69, No. 2, 284–288, Feb. 2022.

[13] Pozar, D. M., *Microwave Engineering: Theory and Techniques*, 4th ed., John Wiley & Sons, New York, NY, USA, 2011.

[14] Huang, Z., Y. Cheng, and Y. Zhang, "Dual-mode dielectric waveguide filters with controllable transmission zeros," *IEEE Microwave and Wireless Components Letters*, Vol. 31, No. 5, 449–452, May 2021.

[15] Tang, W. S., M. Li, Y.-M. Zhang, and S. Y. Zheng, "Compact dielectric waveguide filters with controllable transmission zeros using dual external coupling and hybrid ridge and post," *IEEE Transactions on Microwave Theory and Techniques*, Vol. 72, No. 11, 6574–6584, Nov. 2024.

[16] Xu, Z., Y. Wu, Q. Dong, and W. Wang, "Miniaturized dual-band filter using dual-mode dielectric waveguide resonator," *IEEE Microwave and Wireless Components Letters*, Vol. 32, No. 12, 1411–1414, Dec. 2022.

[17] Wang, Z., Y. Wu, Z. Xu, Y. Yao, and W. Wang, "Flexible dual-band dielectric waveguide filter based on degenerate modes," *IEEE Microwave and Wireless Technology Letters*, Vol. 34, No. 7, 887–890, Jul. 2024.

[18] Wang, Z., Y. Wu, Z. Xu, Y. Yao, and W. Wang, "Adjustable triple-band triple-mode dielectric waveguide filter with multiple transmission zeros," *IEEE Microwave and Wireless Technology Letters*, Vol. 34, No. 6, 619–622, Jun. 2024.

[19] Chen, X.-P. and K. Wu, "Substrate integrated waveguide cross-coupled filter with negative coupling structure," *IEEE Transactions on Microwave Theory and Techniques*, Vol. 56, No. 1, 142–149, Jan. 2008.

[20] Zakharov, A., "Transmission zeros of trisection and quadruplet bandpass filters with mixed cross coupling," *IEEE Transactions on Microwave Theory and Techniques*, Vol. 69, No. 1, 89–100, Jan. 2021.

[21] Zhou, Y.-K., W. Qin, W.-W. Yang, and J.-X. Chen, "Multiband dielectric waveguide bandpass filters based on frequency mapping technique," *IEEE Transactions on Microwave Theory and Techniques*, Vol. 73, No. 2, 1062–1072, Feb. 2025.

[22] Yao, X., Y. Wang, Y. Gao, and J. Zhang, "Novel hexagonal cross-coupled dielectric waveguide filter," *Progress In Electromagnetics Research C*, Vol. 152, 253–258, 2025.